Atmos. Chem. Phys. Discuss., 10, 27283–27320, 2010
www.atmos-chem-phys-discuss.net/10/27283/2010/
doi:10.5194/acpd-10-27283-2010

Atmospheric
Chemistry
and Physics
Discussions

Understanding the transport of Patagonian dust and its influence on marine biological activity in the South Atlantic Ocean

M. S. Johnson[1], N. Meskhidze[1], V. P. Kiliyanpilakkil[1], and S. Gassó[2]

[1]Marine Earth and Atmospheric Science, North Carolina State University, Raleigh, NC, USA
[2]Goddard Earth Space and Technology, University of Maryland Baltimore County and NASA, Greenbelt, Maryland, USA

Received: 2 September 2010 – Accepted: 29 October 2010 – Published: 10 November 2010

Correspondence to: N. Meskhidze (nmeskhidze@ncsu.edu)

Published by Copernicus Publications on behalf of the European Geosciences Union.

Abstract

The supply of bioavailable iron to the high-nitrate low-chlorophyll (HNLC) waters of the Southern Ocean through atmospheric pathways could stimulate phytoplankton blooms and have major implications for the global carbon cycle. In this study, model results and remotely-sensed data are analyzed to examine the horizontal and vertical transport pathways of Patagonian dust and quantify the effect of iron-laden mineral dust deposition on marine biological productivity in the surface waters of the South Atlantic Ocean (SAO). Model simulations for the atmospheric transport and deposition of mineral dust and bioavailable iron are carried out for two large dust outbreaks originated at the source regions of Northern Patagonia during the austral summer of 2009. Model-simulated horizontal and vertical transport pathways of Patagonian dust plumes are in reasonable agreement with remotely-sensed data. Simulations indicate that the synoptic meteorological patterns of high and low pressure systems are largely accountable for dust transport trajectories over the SAO. According to model results and retrievals from the Cloud-Aerosol Lidar and Infrared Pathfinder Satellite Observations (CALIPSO), synoptic flows caused by opposing pressure systems (a high pressure system located to the east or north-east of a low pressure system) elevate the South American dust plumes well above the marine boundary layer. Under such conditions, the bulk concentration of mineral dust can quickly be transported around the low pressure system in a clockwise manner, follow the southeasterly advection pathway, and reach the HNLC waters of the SAO and Antarctica in ~3–4 days after emission from the source regions of Northern Patagonia. Two different mechanisms for dust-iron mobilization into a bioavailable form are considered in this study. A global 3-D chemical transport model (GEOS-Chem), implemented with an iron dissolution scheme, is employed to estimate the atmospheric fluxes of soluble iron, while a dust/biota assessment tool (Boyd et al., 2010) is applied to evaluate the amount of bioavailable iron formed through the slow and sustained leaching of dust in the ocean mixed layer. The effect of iron-laden mineral dust supply on surface ocean biomass is investigated by comparing predicted surface chlorophyll-*a* concentration ([Chl-*a*]) to remotely-sensed data. As the dust transport episodes examined here represent large summertime outflows of mineral dust from South American continental sources, this study suggests that (1) atmospheric fluxes of mineral dust from Patagonia are not likely to be the major source of bioavailable iron to ocean regions characterized by high primary productivity; (2) even if Patagonian dust plumes may not cause visible algae blooms, they could still influence background [Chl-*a*] in the South Atlantic sector of the Southern Ocean.

1 Introduction

Iron (Fe) is one of the nutrient elements needed by phytoplankton to carry out photosynthesis. Despite being the fourth most abundant element in the Earth's crust, Fe is in a short supply in most near-surface remote oceanic waters. Concentrations of Fe are particularly low in the so called high-nitrate low-chlorophyll (HNLC) oceanic regions, where availability of the micronutrient Fe has been shown to be a limiting factor for marine primary productivity (Martin and Gordon, 1988; Martin and Fitzwater, 1988; Martin, 1990). There are three main HNLC regions (subarctic North Pacific, east Equatorial Pacific, and the Southern Ocean), with the Southern Ocean (SO) suggested to be the most biogeochemically significant due to its large spatial extent and considerable influence on the global carbon cycle (Martin, 1990; Watson et al., 2000; Boyd et al., 2000; Sarmiento et al., 2004). Mesoscale Fe enrichment experiments have unequivocally shown that the Fe supply in the SO exerts control on the dynamics of plankton blooms, which in turn affect the biogeochemical cycles of carbon, nitrogen, silicon, sulfur, and ultimately influences the Earth's climate system (e.g., Boyd et al., 2007).

The atmospheric deposition of aeolian dust is one of the natural pathways for the contribution of Fe to the surface waters of the SO. Compared to other Fe-limited regions, the SO is thought to receive the lowest flux of dust-Fe (Duce and Tindale, 1991) and, as a result, upwelling of deep water, re-suspension of sediments, re-mineralization of sinking material, diffusion from the pore waters, and release of bioavailable Fe from glaciers and icebergs have often been proposed to be the likely suppliers of Fe to this region (de Baar et al., 1995; Löscher et al., 1997; Watson et al., 2000; Raiswell et al., 2008). However, over the past decade there has been a growing interest for the possible role of mineral dust-Fe in regulating this region's biological productivity, air-sea fluxes of carbon dioxide (CO_2), emissions of marine biogenic aerosols and trace gases, and overall global climate (Martin and Fitzwater, 1988; Martin, 1990; Zhuang et al., 1992; Jickells et al., 2005; Meskhidze et al., 2007; Ito and Kawamiya, 2010). Based on a significant positive correlation between the atmospheric delivery of mineral dust and phytoplankton growth in the surface waters of the SO, downwind from the Patagonian and Southern Australian regions (Gabric et al., 2002; Erickson et al., 2003) it was proposed that phytoplankton productivity in the South Atlantic Ocean (SAO) is controlled by Patagonian dust deposition (Erickson et al., 2003). However, recent studies have pointed out that dust-Fe deposition to the surface waters of the SO could be less important for primary productivity than previously estimated (Meskhidze et al., 2007; Blain et al., 2007, 2008; Wagener et al., 2008; Boyd et al., 2010) and that the ocean Fe fertilization alone may not account for atmospheric CO_2 reduction enough to significantly alter the course of climate (e.g., Denman, 2008; Buesseler et al., 2008; Mackie et al., 2008; Strong et al., 2009). Despite the potentially important role of Fe-laden dust deposition on marine primary productivity and atmosphere-ocean CO_2 fluxes, few studies exist that can help constraining the deposition of bioavailable Fe and subsequent changes in surface ocean chlorophyll concentration and carbon sequestration rates in the polar and sub-polar waters of the SO. To understand the biogeochemical cycling of Fe in both present and past climate regimes and the role of mineral dust in Fe-mediated carbon sequestration in the SO, researchers have looked at the detailed stratigraphic records of mineral dust in Antarctic ice cores and used them as proxies for paleoclimate and paleowinds (e.g., Delmonte et al., 2004; Lambert et al., 2008). When making connections between past glacial-interglacial fluctuations in dust deposition to Antarctica and carbon dynamics in the SO, in addition to particular sources and deposition processes (e.g., Petit et al., 1999; Lambert et al., 2008), it is important to properly quantify the transport pathways (Krinner and Genthon, 2003; Krinner et al., 2010; Li et al., 2008, 2010), bioavailable portion of mineral-Fe (Jickells et al., 2005; Meskhidze et al., 2003, 2005; Solmon et al., 2009), and the fraction of fixed carbon sequestered to the deep oceans (>250 m) (e.g., Buesseler et al., 2004).

Several studies that have been conducted to quantify dust transport pathways and deposition fluxes in the Southern Hemisphere (SH) seem to agree that the arid and semi-arid regions of South America and Australia are the major source regions for aeolian dust deposited to the SO (Fung et al., 2000; Ginoux et al., 2001; Prospero et al., 2002; Zender et al., 2003; Li et al., 2008). Although, there is no definite agreement, modeling and remote sensing studies have also identified distinct horizontal and vertical transport pathways for South American and Australian dust sources over the SO. South American dust has been shown to largely remain at lower elevations (below 6 km), while Australian dust is likely to be elevated to higher levels of the free troposphere (Krinner and Genthon, 2003; Gassó and Stein, 2007; Li et al., 2008; Krinner et al., 2010; Gassó et al., 2010). The bioavailable fraction of Fe in Southern Hemispheric dust (e.g., South America) remains a topic of active debate (Cassar et al., 2007; Boyd and Mackie, 2008). Recent modeling studies have shown that due to the pristine nature of this region, the water soluble (or bioavailable) fluxes of Fe (sol-Fe) in mineral dust over the SO could be much lower compared to Northern Hemispheric dust (Meskhidze et al., 2007; Johnson et al., 2010). Quantification of the climatic role of South American dust is further complicated by the fact that the proposed fraction of the fixed carbon sequestered to the deep oceans varies by up to a factor of ∼200 (e.g., de Baar et al., 2008), making the link between marine primary productivity and carbon removal extremely difficult.

Using model simulations and remotely-sensed data, this study attempts to better quantify the role of aeolian dust-Fe supply for marine ecosystem productivity in the SAO domain of the SO. Dust transport pathways and deposition fluxes, resulted changes in ocean ecosystem productivity, and the potential effect of dust-Fe deposition on carbon sequestration in this region are examined based on two large dust advection episodes from South America. Here the SAO is roughly defined as the part of the Atlantic Ocean between the equator and the Antarctic coastline (from north to south) and from 70° W to 20° E, and the possible HNLC region as the portion of SAO south of the Antarctic Circumpolar Current (ACC) (~42° S) (Boyd et al., 2007).

2 Methods

2.1 GEOS-Chem/DFeS

The three dimensional global chemistry transport model GEOS-Chem (v8-01-01) was used in this study to simulate Patagonian dust transport and deposition to the SAO. The model uses GEOS-5 meteorological fields (Bey et al., 2001; Park et al., 2004; Evans and Jacob, 2005) at a 2°×2.5° (latitude-longitude) grid resolution and 47 vertical levels. For the prognostic calculations of Fe dissolution, the model is run with a full chemistry configuration, which includes H_2SO_4-HNO_3-NH_3 aerosol thermodynamics coupled to an O_3-NO_x-hydrocarbon-aerosol chemical mechanism (Bey et al., 2001; Park et al., 2004). The emissions and chemistry of sulfur compounds, carbonaceous aerosols, and sea-salt are described by Park et al. (2004), Heald et al. (2004), and Alexander et al. (2005), respectively. To simulate dust mobilization, GEOS-Chem combines the Dust Entrainment and Deposition (DEAD) scheme (Zender et al., 2003) with the source function used in the Goddard Chemistry Aerosol Radiation and Transport (GOCART) model (Ginoux et al., 2001; Chin et al., 2004). Principal source regions are deserts or dry lakes and streambeds where alluvial deposits have accumulated. Mineral dust mobilization occurs when turbulent drag forces of the atmosphere overcome gravitational inertia and inter-particle cohesion. Once mineral dust is mobilized from the surface, the model uses four standard dust bins with diameter boundaries of 0.2–2.0, 2.0–3.6, 3.6–6.0 and 6.0–12.0 µm to simulate global dust transport and deposition (Fairlie et al., 2007).

In order to determine the influence of mineral dust from Patagonia on biological productivity in the SAO, GEOS-Chem was modified to treat a number of individual dust source regions separately. The terrestrial portion of the globe was divided into seven major dust source regions (i.e., North Africa, South Africa, North America, Asia, Australia, the Middle East, and South America) (Prospero et al., 2002). Dust emission fluxes, calculated for each source region, were assigned separate tracers. Such treatment allowed dust from each of the seven regions to be independently transported, chemically transformed, and removed from the atmosphere. GEOS-Chem with the modified dust scheme gave us the opportunity to estimate the relative contribution of each of the seven dust regions to total atmospheric dust and bioavailable Fe fluxes to the SAO domain. The fluxes of sol-Fe to the ocean were calculated using GEOS-Chem with a prognostic dust-Fe dissolution scheme (GEOS-Chem/DFeS model) (Solmon et al., 2009; Johnson et al., 2010). GEOS-Chem/DFeS simulations of South American dust were shown to be in reasonable agreement with available surface and remotely-sensed data (Johnson et al., 2010).

2.2 Bioavailable portion of mineral-Fe and the ocean productivity

In addition to model-predicted fluxes of water soluble iron produced during atmospheric transport and transformation of mineral dust (the so-called "rapidly released" fluxes of sol-Fe), throughout its residence time in the surface ocean dust can also become a source of bioavailable Fe due to the slow and sustained leaching of mineral-Fe (Boyd et al., 2010). To calculate the amount of sol-Fe leached from mineral dust we adopt the formulation of Boyd et al. (2010):

$$\mathrm{Fe}_{\mathrm{Leachable}}=\frac{\mathrm{DST}\cdot f_{\mathrm{Fe}}\cdot f_{\mathrm{Fe}_{\mathrm{Leachable}}}}{r_{\mathrm{Leachable}}\cdot t_{\mathrm{residence}}\cdot D} \tag{1}$$

where $\mathrm{Fe}_{\mathrm{Leachable}}$ is the amount of Fe leached in the surface ocean for a given quantity of mineral dust deposition ($\mathrm{g\,m^{-3}}$), DST is GEOS-Chem/DFeS-predicted mineral dust deposition during a given dust episode ($\mathrm{g\,m^{-2}}$), f_{Fe} is the average mass fraction of

Fe in mineral dust (3.5%) (Duce and Tindale, 1991), $f_{\mathrm{Fe}_{\mathrm{leachable}}}$ is the fraction of Fe in deposited dust that is leachable, $r_{\mathrm{Leachable}}$ is the rate of Fe leaching (30 day^{-1}), $t_{\mathrm{residence}}$ is the residence time of dust in the ocean mixed layer (30 day), and D is the monthly-mean mixed layer depth (m). The values for $f_{\mathrm{Fe}_{\mathrm{leachable}}}$, $r_{\mathrm{Leachable}}$, and $t_{\mathrm{residence}}$ are taken from Boyd et al. (2010) and the value for D was obtained from the global climatological monthly-averaged mixed layer depth data (2°×2°) (de Boyer Montégut et al., 2004) and regridded to a 0.25°×0.25° resolution.

Assuming the model-predicted atmospheric fluxes of mineral-Fe is the limiting micronutrient for phytoplankton productivity in the HNLC waters of the SAO, we can convert fluxes of sol-Fe to increases in surface Chlorophyll-*a* concentration ([Chl-*a*]) and use that as a reliable proxy for the surface ocean primary production (Meredith et al., 2003). The magnitude of [Chl-*a*] production per unit time (in mg m^{-3} day^{-1}) due to atmospheric fluxes of bioavailable Fe can be calculated as:

$$\frac{d[\mathrm{Chl}\text{-}a]}{dt} = \frac{12\,000 \cdot \mathrm{sol\text{-}Fe} \cdot (\mathrm{C:Fe}) \cdot (\mathrm{Chl}\text{-}a:\mathrm{C})}{D} \tag{2}$$

where the constant of 12 000 is used for a unit conversion (from mol C to mg C), sol-Fe represents the model-predicted atmospheric fluxes of soluble Fe (mol m^{-2} day^{-1}), C:Fe is the carbon to Fe ratio characteristic for the major phytoplankton species found in the enhanced productivity regions of the SAO (mol mol^{-1}), and Chl-*a*:C is the chlorophyll-*a* to carbon ratio in phytoplankton (mg mg^{-1}). Table 1 summarizes the values (with corresponding references) for the parameters used in Eq. (2). This equation implicitly assumes that all of the bioavailable Fe (either from the atmospheric deposition of sol-Fe or the leaching of mineral dust particles) will contribute to chlorophyll production in the HNLC waters of the SO. Such a provision is supported by past mesoscale Fe enrichment experiments and results from previous literature studies on marine biota and Fe interactions in HNLC waters (e.g., Hutchins et al., 1999; Tsuda et al., 2003; Jin et al., 2008; Lancelot et al., 2009).

2.3 Satellite data

In this study, GEOS-Chem-predicted mineral dust transport during the two dust outbreak episodes of 23–30 January 2009 and 11–18 February 2009 (from here on J23 and F11) were compared to real-time imagery and remotely-sensed data obtained from Terra and Aqua Moderate Resolution Imaging Spectroradiometer (MODIS) retrievals (Kaufman et al., 1997; Tanré et al., 1997; Remer et al., 2005) and the Cloud-Aerosol Lidar and Infrared Pathfinder Satellite Observation (CALIPSO) (Vaughan et al., 2004). Real-time imagery from the MODIS Rapid Response system (http://rapidfire.sci.gsfc.nasa.gov/gallery/) was used for the visual confirmation of mineral dust outbreaks from South American continental sources.

The model-predicted vertical profiles of Patagonian dust concentrations were compared to CALIPSO Level 2 (v3.01) data (http://eosweb.larc.nasa.gov/PRODOCS/calipso/table_calipso.html). The CALIPSO algorithm is distinctive from other satellite algorithms in its capability to discriminate dust aerosols (desert dust and polluted dust) from other subtypes such as clean continental, marine, polluted continental and smoke. To determine the aerosol subtypes the algorithm uses volume depolarization ratio, integrated attenuated backscatter, the earth surface types (land/ocean), and the layer altitude information. The aerosol optical depth (AOD) and extinction/backscatter profile retrievals for different particle subtypes require aerosol extinction-to-backscatter ratio (lidar ratio) specific to the above mentioned six aerosol types (Omar et al., 2009; Young and Vaughan, 2009). The Cloud-Aerosol Lidar with Orthogonal Polarization (CALIOP) identified features are classified into aerosol and cloud using a cloud-aerosol discrimination (CAD) algorithm. The CAD algorithm separates clouds and aerosols and provides the cloud-aerosol discrimination score for each layer (Liu et al., 2009). The standard CAD scores for the level of confidence in the aerosol-cloud classification are ranging from −100 to 0 for aerosol and +100 to 0 for cloud. A larger absolute value of the CAD score indicates higher confidence of the feature classification. To get relatively high confidence cloud free data, different aerosol types and the corresponding

AODs are extracted using CAD scores of −20 to −100 (Yu et al., 2010) for the conditions when initial lidar ratio (selected based on type and subtype of the layer) is equal to the final lidar ratio (derived by applying transmittance correction to the extinction processing) (http://eosweb.larc.nasa.gov/PRODOCS/calipso/Quality_Summaries/).

Daily-averaged Level 3 data for [Chl-*a*] at $\frac{1}{12}^\circ \times \frac{1}{12}^\circ$ resolution were obtained from the Sea-viewing Wide Field-of-view Sensor (SeaWiFS) (version 5.1) (O'Reilly et al., 1998) and regridded to 0.25°×0.25°. Previous studies have shown that fluctuations in daily surface [Chl-*a*] retrievals by SeaWiFS compare well with in situ measurements in the SAO, with some possible underestimations in the Drake Passage and Scotia Sea regions of the Antarctic basin (Gregg and Casey, 2004; Dogliotti et al., 2009).

3 Results

3.1 Mineral dust transport from Patagonia

Dry lake/river beds and low lying regions in Patagonia with little vegetative cover are the predominant source regions of windblown dust emanating from the South American continent and deposited to the surface waters of the SAO (Prospero et al., 2002; Li et al., 2008; Wagener et al., 2008; Johnson et al., 2010). Patagonian dust plumes have been suggested to travel at low altitudes over the SAO and are accompanied by large amounts of cloud cover (Gassó and Stein, 2007; Li et al., 2008; Krinner et al., 2010), making it difficult to be detected by satellites. On 23 January 2009 and 17 February 2009 clear images of mineral dust transport were captured by Aqua MODIS (see Fig. 1) allowing for the rare opportunity to carry out model analysis of dust transport for episodes with visual confirmation of mineral dust advection from the South American continent. Figure 1a,b indicates that mineral dust emission regions are located near San Antonio Oeste, a region that was previously identified as one of the largest dust sources in Patagonia (Johnson et al., 2010). This region is located in the northern end of Patagonia and it has become an active dust source since 2008 likely due to a combination of poor livestock management and drought conditions (Geist and Lambin, 2004; McConnell et al., 2007). According to Fig. 1, GEOS-Chem-predicted transport pathways over the ocean are generally comparable with the satellite images, although the agreement between model-predictions and satellite imagery is somewhat poorer for 17 February 2009, when dust originated from three individual small sources. Model simulations show, that both the J23 and F11 outbreaks had similar transport pathways over the SAO, with column dust concentrations for the F11 dust storm roughly a factor of four higher compared to the J23 dust event (see Fig. 1). In addition to horizontal transport, existence of CALIPSO retrievals gives the unique opportunity for examining model-predicted vertical transport pathways of Patagonian dust. Unfortunately, out of the two dust episodes with clear visual evidence of long-range transport, CALIPSO data is only available for the J23 episode; therefore only the J23 dust storm will be discussed in detail.

In order to examine the impact of synoptic meteorology on mineral dust transport, previous studies have applied sea level pressure anomalies (SLPAs) as a proxy for high and low pressure systems (e.g., Liang et al., 2005; Yang et al., 2007). Figure 2 compares the spatial patterns of the model-predicted column abundance of mineral dust and GEOS-5 SLPAs over the SAO for 23–25 January 2009. This figure indicates that the relative positioning of high and low pressure systems may control the south-eastward transport of the J23 dust plume (Southern Hemispheric low pressure systems rotate clockwise and high pressure systems rotate counter-clockwise). Analyses of model simulations suggest that synoptic flows caused by opposing pressure systems (a high pressure system located to the east/north-east of a low pressure system) produce large-scale southerly advection between 40° S and 60° S. The bulk concentration of mineral dust follows the southerly advection pathway and gets transported over the HNLC waters of the SAO and East Antarctica. The controlling effect of horizontal transport pathways of Patagonian dust by synoptic meteorological patterns found over the SAO is consistent with the results of the recent study by Li et al. (2010).

In addition to horizontal transport, the location of high and low pressure systems may also influence the vertical structure of Patagonian dust plumes. Figures 3–5 compare GEOS-Chem-predicted column concentrations and vertical profiles of mineral dust for the J23 dust plume to CALIPSO aerosol type and dust AOD retrievals for 23–25 January 2009. Notice, that GEOS-Chem outputs are daily-averaged data while CALIPSO results are for a specific overpass time. Figures 3 and 4 show that near the South American continent, both GEOS-Chem predictions and CALIPSO retrievals position the J23 dust plume at a low altitude (below 2–3 km). Although CALIPSO puts the major portion of the dust plume slightly north to that of GEOS-Chem, the model-simulated vertical structure of the J23 plume compares relatively well with CALIPSO AOD data (Figs. 3b,c and 4b,c). Detailed analysis of model simulations reveal that after leaving the continent, the Patagonian dust plume encountered a strong cyclone over the SAO. On 24 January 2009 when the dust plume was about to enter the western sector of the large low pressure system (~20° W), the bulk of the dust was still located below 3 km over the SAO (Fig. 4b). As the plume entered the cyclone on 25 January 2009 (Fig. 5), mineral dust gets transported around the low pressure system in a clockwise manner. Although simulations are in poorer agreement with the CALIPSO retrievals on 25 January, both model results (Figs. 5c,f) and satellite overpasses (Figs. 5b,e) show that over the northern sector of the cyclone (~0° W–5° E) the dust plume was lifted above the marine boundary layer (MBL) and got diluted vertically in the free troposphere (up to ~6 km). It should also be noticed that in the 2–3 days of transport time over the SAO the dust plume is significantly depleted and the comparison of remotely-sensed data (for specific overpass time) and the daily-averaged model results become less reliable. Overall, our model simulations suggest that synoptic meteorological conditions played a considerable role in both the horizontal and vertical advection of the J23 storm over the SAO. By using the combination of model and remote sensing techniques, we have shown that low pressure systems can elevate Patagonian dust to heights suitable for long-range transport over the SAO.

Further analyses of model simulations for the J23 and F11 dust episodes revealed two main transport pathways for mineral dust emitted from the northern end of Patagonia and advected over the SAO. Figure 6 shows that when a high pressure system is located to the east/north-east of a low pressure system, it can effectively block the strong easterlies. Under such conditions, Northern Patagonian dust plume trajectories will go around the low pressure system in a clockwise manner and follow a south-eastward direction. Under such conditions, both model-simulations and CALIPSO retrievals suggest that dust plumes can be uplifted and diluted vertically in the free troposphere creating suitable conditions for the long-range transport towards East Antarctica. A clear example of this southerly advection is seen on 25 January (Fig. 6a–c). However, when an intense high pressure system is located north/north-west of a low pressure system over the SAO, Northern Patagonian dust follows an anticyclonic circulation and gets transported in an easterly/north-easterly direction. No significant dust uplift is observed for such an advection pathway. Interestingly, during the F11 dust episode both transport routes become evident. Between 13–14 February 2009 the Patagonian dust plume is transported to the south-east as the SAO is dominated by a low pressure system with a high pressure system to the east/north-east (Fig. 6d,e), while on 15 February 2009 as the low pressure weakens, the dust plume gets entrained into the anticyclonic circulation and gets advected to the east/north-east, following the synoptic flow (Fig. 6f). Although here we show dust trajectories for only two individual dust episodes, results of this study are consistent with the recent work of Li et al. (2010), suggesting that synoptic patterns of high and low pressure systems over the SAO can have considerable influence on Patagonian dust transport trajectories.

The explicit contribution of Patagonian source regions to total dust deposited to the SAO during the J23 and F11 dust episodes were examined using the modified version of GEOS-Chem, with seven specific dust source regions. Figure 7 shows that during the J23 and F11 dust episodes Patagonian sources likely accounted for the majority of dust deposited to the South Atlantic Sector of the SO. This result is in agreement with recent studies (e.g., Li et al., 2008, 2010; Bory et al., 2010), suggesting that the transport and deposition of dust from Patagonia represents the major pathways for the atmospheric fluxes of the micronutrient Fe to the HNLC surface waters of the SAO. Model calculations show that during the J23 and F11 dust episodes a total of ∼1.0 and 4.0 Tg of dust was deposited to the SAO oceanic regions, respectively. Roughly ∼40% of this mineral dust got deposited to the proposed HNLC region. Figure 7 also demonstrates that during the austral summer mineral dust from Patagonia can be transported over thousands of kilometers reaching the west coast of South Africa and Australia and the East and West Antarctic continent. However, notice that the considerable contribution of Patagonian sources to mineral dust fluxes seen on Fig. 7 are largely due to the absence of other dust sources during this time and gives no indication about the actual amount of mineral dust deposition to the SAO. The contribution of Patagonian sources to dust deposition in the Pacific sector of the SO is quickly declining to near zero values due to the strong contribution from dust sources in Australia.

3.2 Response of marine biological productivity to mineral dust deposition

The potential interactions between mineral dust deposition and marine biological productivity during the J23 and F11 dust events was explored using GEOS-Chem/DFeS-predicted daily-averaged sol-Fe deposition (regridded to $0.25^\circ \times 0.25^\circ$ to match the resolution of remotely-sensed SeaWiFS data) and offline calculations for the amount of Fe leached from mineral dust during its mixed layer residence time. The expected [Chl-*a*] production due to the atmospheric deposition of sol-Fe was calculated using Eq. (2). Eight-day periods were chosen for each dust event in order to capture the possible biological response to the initial supply of sol-Fe-laden dust deposited to the SAO. Artificial mesoscale Fe-enrichment experiments revealed that in the SO [Chl-*a*] production responds rapidly to Fe supply (∼3–5 days) (e.g., Boyd et al., 2004, 2007), therefore this length of time should be suitable for capturing the initial response of marine biota due to the supply of Fe-laden dust. When using average values of the different parameters of Table 1, the model-predicted atmospheric fluxes of sol-Fe during the J23 and F11 dust episodes should have increased surface [Chl-*a*] (Δ[Chl-*a*]$_{\mathrm{pred}}$) between

0.001 and 0.7 mg m^{-3} (see Fig. 8). Such predicted changes in [Chl-*a*] are small for the SAO, where algal blooms with [Chl-*a*] on the order of several mg m^{-3} have often been reported (e.g., Korb et al., 2004; Romero et al., 2006; Blain et al., 2007). However, as the phytoplankton productivity in surface waters of the SAO are generally considered to be limited by the availability of Fe, even small additions of bioavailable Fe from mineral dust could influence primary productivity in this region. To estimate potential contribution of atmospheric fluxes of bioavailable Fe to phytoplankton productivity in the SAO for both the J23 and F11 episodes, we have compared $\Delta[\text{Chl-}a]_{\text{pred}}$ (Figs. 8a,b) to the differences in remotely-sensed 8-day averaged [Chl-*a*] ($\Delta[\text{Chl-}a]_{\text{obs}}$) values (after the storm minus before the storm). Figure 9a,b shows that there are large areas near the dust deposition regions where $\Delta[\text{Chl-}a]_{\text{obs}}$ changes by more than 0.5 mg m^{-3} (i.e., phytoplankton blooms easily visible from the satellites). However, comparison of Fig. 8a,b to Fig. 9c,d indicates that the contribution of model-predicted mineral dust to marine productivity in the SAO is disproportionately larger in regions with minimal $\Delta[\text{Chl-}a]_{\text{obs}}$. Figure 10 further shows that for both the J23 and F11 episodes the ratio $\Delta[\text{Chl-}a]_{\text{pred}}/\Delta[\text{Chl-}a]_{\text{obs}}$, a proxy for the contribution of model-predicted sol-Fe to biological productivity in the HNLC regions of the SAO, decreases sharply for the larger values of $\Delta[\text{Chl-}a]_{\text{obs}}$. Figure 10 shows that atmospheric fluxes of sol-Fe, while influencing surface ocean productivity in large areas of SAO, played a negligible role in regions with $\Delta[\text{Chl-}a]_{\text{obs}} > 1.0$ mg m^{-3}. Analysis of data shown on Fig. 10 revealed that as much as 50% of all the data points in HNLC waters of the SAO with $\Delta[\text{Chl-}a]_{\text{obs}} > 0$ had over 20% contribution from mineral dust. This result indicates that the large number of the remotely sensed grid cells with increasing [Chl-*a*] during J23 and F11 dust storms had sizable contribution from atmospheric fluxes of Fe. However, these grid cells only accounted for <30% of the total marine biological productivity in this region. To the extent that carbon export from surface waters of the SAO is believed to be primarily controlled by large, rapidly-sinking diatoms, capable of producing visible blooms (de Baar et al., 1995, 2008), this result suggests that Patagonian dust fluxes may only have a modest influence on the SO carbon cycle.

There are, however, a number of caveats in our calculations that need to be addressed. Model sensitivity studies of Johnson et al. (2010) show that uncertainties in simulated fluxes of sol-Fe to the surface waters of the SAO are large. Dust deposition rates, dissolution of different Fe-laden minerals, and chemical and mineralogical composition of Patagonian dust can contribute over 60% uncertainty in simulated sol-Fe fluxes. Uncertainties in reported values of C:Fe and Chl-*a*:C ratios (see Table 1), and the SAO ocean mixed layer depth (see Table 1), could also add considerable uncertainties to model-predicted changes in marine productivity. In addition to atmospheric fluxes of sol-Fe associated with the chemically aged mineral dust in the atmosphere (so-called rapidly-released Fe), it has been suggested that a considerable amount of bioavailable Fe can also be leached from mineral dust during its mixed layer residence time. This leaching dissolution mechanism comprises processes such as grazer/particle interactions, photo-reductive mechanisms in conjunction with siderophores, and reduction of mineral-Fe within particle micro-zones (Boyd et al., 2010). Calculations using Eq. (1) show that for both the J23 and F11 dust episodes the amount of bioavailable Fe leached over the period of 30 days (assumed mixed layer residence time in the SAO, Boyd et al., 2010) contributed on average ∼50% of rapidly released Fe. When all the uncertainties in model-predicted [Chl-*a*] are considered (with the exception of mixed layer depth), the maximum value of $\Delta[\text{Chl-}a]_{\text{pred}}$ increased by roughly a factor of 4. The solid red line on Fig. 10 shows the best-fit for the ratio of $\Delta[\text{Chl-}a]_{\text{pred}}/\Delta[\text{Chl-}a]_{\text{obs}}$ using the estimated uncertainties in model-predicted [Chl-*a*]. Therefore, the shaded area under the curve can be viewed as a probable contribution of Patagonian dust fluxes to marine productivity in the surface waters of the HNLC regions of the SAO. Figure 10 shows that due to the large uncertainties associated with the key parameters used in Eqs. (1) and (2), and the processes for the supply of sol-Fe to the surface waters of SAO by atmospheric pathways, the role of Patagonian dust in surface biological productivity and carbon dynamics of the SO cannot be fully ascertained. This result highlights the great need for more detailed research of marine biota/mineral-dust interactions in the SAO.

4 Conclusions

Two large dust outbreaks from Patagonia (23–30 January 2009, J23 and 11–18 February 2009, F11) were examined in this study to evaluate horizontal and vertical transport pathways of South American dust and quantify the impact of enhanced mineral dust and sol-Fe fluxes on marine biological productivity in the surface waters the SAO. The global chemistry transport model GEOS-Chem/DFeS was used to reveal the processes that define the horizontal and vertical transport pathways of Northern Patagonian dust over the SAO and estimate the potential effect of mineral dust and sol-Fe deposition on biological activity in HNLC waters of the SAO. Retrievals of remotely sensed surface [Chl-*a*] before and after the large summertime outflows of mineral dust allow us to estimate potential contribution of mineral dust to surface ocean primary productivity in the SAO.

Analyses of model results and remotely-sensed data revealed that Northern Patagonian dust can travel long distances over the SAO. The long-range transport shown during this study is consistent with recent works of McConnell et al. (2007), Gassó et al. (2010) and Li et al. (2010) which demonstrate that Patagonian dust can travel thousands of kilometers away from the South American continent reaching the coast of South Africa and West and East Antarctica. As the dust outflow off the coast of South America typically occurs below 2 km, for mineral dust to get transported over such long distances, the dust plumes need to be elevated to heights above the MBL. Model simulations revealed that the horizontal and vertical pathways of Northern Patagonian dust are highly dependent on the synoptic meteorological patterns of strong high and low pressure systems over the SAO. When a high pressure system is located to the east/north-east of a low pressure system, Northern Patagonian dust plume trajectories will go around the low pressure system in a clockwise manner and get preferentially transported in a southerly/south-easterly direction. However, when a high pressure system is located to the north/north-west of a low pressure system, Northern Patagonian dust follows an anticyclonic circulation and gets transported in an easterly/north-easterly direction. Model simulations and remote sensing also revealed that as the plume enters the cyclonic system rotating in a clockwise manner, the dust plume can be rapidly lifted above the MBL and diluted vertically in the free troposphere (up to ~6 km). A similar process was reported in a satellite observation made by Gassó and Stein (2007) which demonstrated Patagonian dust being uplifted as it encountered a low pressure center over the SAO. Such elevations are suitable for Fe-laden mineral dust to be transported long distances, often reaching the HNLC regions of the SAO and East Antarctica.

The potential effect of bioavailable Fe deposition on phytoplankton dynamics in the SAO during the J23 and F11 dust episodes was explored using model-predicted fluxes of sol-Fe delivered to HNLC waters of the SAO through atmospheric pathways (so-called rapidly released fluxes of sol-Fe). In addition to atmospheric fluxes of sol-Fe, we have used a dust/biota assessment tool (Boyd et al., 2010) to estimate the amount of bioavailable Fe leached from mineral dust during its residence time in the surface waters of the SAO. Offline calculations of [Chl-*a*] enrichments due to predicted amounts of sol-Fe were compared to remotely-sensed SeaWiFS satellite data and used as an indirect assessment of Patagonian dust contribution to phytoplankton dynamics in the SAO. Our calculations indicate that on average the atmospheric supply of Fe-laden dust has a disproportionate effect on surface [Chl-*a*]. Contribution of dust-laden Fe to biological productivity in the SAO decreases sharply for areas with sizable variation in remotely-sensed [Chl-*a*]. This result implies that in surface waters of the SAO that can sustain large increases in marine primary productivity, the majority of the bioavailable Fe is delivered through non-atmospheric pathways (e.g., upwelling of deep water, re-suspension of sediments, re-mineralization of sinking material, diffusion from the pore waters, and release of bioavailable Fe from glaciers and icebergs). As the two dust events examined in this study are believed to be representative of strong summertime dust outflow from Northern Patagonia, and the supply of bioavailable Fe to the SAO is known to strongly favor production of the larger-size, rapidly-sinking diatoms with highest efficiency of carbon removal from the upper ocean, results of this study suggest that Patagonian dust fluxes should have a lesser effect on the SO carbon cycle. However, calculations also revealed that when large uncertainties in GEOS-Chem/DFeS predicted fluxes of sol-Fe, leaching rates of bioavailable Fe from mineral dust, and reported values for C:Fe, Chl-*a*:C ratios are considered, Patagonian dust sources could be responsible for the major fraction of remotely-sensed [Chl-*a*] increases in SAO domain. Due to such large uncertainties associated with model-predicted atmospheric fluxes of bioavailable Fe and the parameters used in our offline calculations of [Chl-*a*], further research is needed to better constrain the interactions between Patagonian dust and marine biota in this Fe-limited region of the SAO.

Acknowledgement. This research was supported by the National Science Foundation through the grant ATM-0826117 and the North Carolina Space Graduate Research Fellowship. Matthew Johnson also acknowledges the opportunity to participate in the Graduate Student Summer Program in Earth System Science at the NASA Goddard Space Flight Center. The authors would like to thank Yongxiang Hu of the NASA Langley Research Center for his help with the processing and application of CALIPSO data. Thanks are also due to Daniel Jacob and the Harvard University Atmospheric Chemistry Modeling Group for providing the basemodel GEOS-Chem used during our research.

References

Alexander, B., Savarino, J., Lee, C. C. W., Park, R. J., Jacob, D. J., Thiemens, M. H., Li, Q. B., and Yantosca, R. M.: Sulfate formation in sea-salt aerosols: Constraints from oxygen isotopes, J. Geophys. Res., 110, D10307, doi:10.1029/2004JD005659, 2005.

Blain, S., Queguiner, B., Armand, L., Sauveur, B., Bombled, B., Bopp, L., Bowie, A., Brunet, C., Brussaard, C., Carlotti, F., Christaki, U., Corbiere, A., Durand, I., Ebersbach, F., Fuda, J., Garcia, N., Gerringa, L., Griffiths, B., Guigue, C., Guillerm, C., Jacquet, S., Jeandel, C., Laan, P., Lefevre, D., Monaco, C. L., Malits, A., Mosseri, J., Obernosterer, I., Park, Y., Picheral, M., Pondaven, P., Remenyi, T., Sandroni, V., Sarthou, G., Savoye, N., Scouarnec, L., Souhaut, M., Thuiller, D., Timmermans, K., Trull, T., Uitz, J., van Beek, P., Veldhuis, M., Vincent, D., Viollier, E., Vong, L., and Wagener, T.: Effect of natural iron fertilization on carbon sequestration in the Southern Ocean, Nature, 446, 1070–1074, doi:10.1038/nature05700, 2007.

Blain, S., Sarthou, G., and Laan, P.: Distribution of dissolved iron during the natural iron fertilisation experiment KEOPS (Kerguelen Island, Southern Ocean), Deep-Sea Res. Pt. II, 55, 594–605, 2008.

Bey, I., Jacob, D. J., Yantosca, R. M., Logan, J. A., Field, B., Fiore, A. M., Li, Q., Liu, H., Mickley, L. J., and Schultz, M.: Global modeling of tropospheric chemistry with assimilated meteorology: model description and evaluation, J. Geophys. Res., 106(D19), 23073–23095, 2001.

Bory, A., Wolff, E., Mulvaney, R., Jagoutz, E., Wegner, A., Ruth, U., and Elderfield, H.: Multiple sources supply eolian mineral dust to the Atlantic sector of coastal Antarctica: evidence from recent snow layers at the top of Berkner Island ice sheet, Earth Planet. Sci. Lett., 291, 138–148, 2010.

Boyd, P. W. and Mackie, D.: Comment on “The Southern Ocean biological response to aeolian iron deposition”, Science, 319, 159, doi:10.1126/science.1149884, 2008.

Boyd, P. W., Watson, A. J., Law, C. S., Abraham, E. R., Trull, T., Murdoch, R., Bakker, D. C. E., Bowie, A. R., Buesseler, K. O., Chang, H., Charette, M., Croot, P., Downing, K., Frew, R., Gall, M., Hadfield, M., Hall, J., Harvey, M., Jameson, G., LaRoche, J., Liddicoat, M., Ling, R., Maldonado, M. T., McKay, R. M., Nodder, S., Pickmere, S., Pridmore, R., Rintoul, S., Safi, K., Sutton, P., Strzepek, R., Tanneberger, K., Turner, S., Waite, A., and Zeldis, J.: A mesoscale phytoplankton bloom in the polar Southern Ocean stimulated by iron fertilization, Nature, 407, 695–702, 2000.

Boyd, P. W., Law, C. S., Wong, C. S., Nojiri, Y., Tsuda, A., Levasseur, M., Takeda, S., Rivkin, R., Harrison, P. J., Strzepek, R., Gower, J., McKay, R. M., Abraham, E., Arychuk, M., Barwell-Clarke, J., Crawford, W., Crawford, D., Hale, M., Harada, K., Johnson, K., Kiyosawa, H., Kudo, I., Marchetti, A., Miller, W., Needoba, J., Nishioka, J., Ogawa, H., Page, J., Robert, M., Saito, H., Sastri, A., Sherry, N., Soutar, T., Sutherland, N., Taira, Y., Whitney, F., Wong, S.-K. E., and Yoshimura, T.: The decline and fate of an iron-induced subarctic phytoplankton bloom, Nature, 428, 549–553, 2004.

Boyd, P. W., Jickells, T., Law, C. S., Blain, S., Boyle, E. A., Buesseler, K. O., Coale, K. H., Cullen, J. J., de Baar, H. J. W., Follows, M., Harvey, M., Lancelot, C., Levasseur, M., Owens, N. P. J., Pollard, R., Rivkin, R. B., Sarmiento, J., Schoemann, V., Smetacek, V., Takeda, S., Tsuda, A., Turner, S., and Watson, A. J.: Mesoscale iron enrichment experiments 1993–2005: synthesis and future directions, Science, 315, 612–617, 2007.

Boyd, P. W., Mackie, D. S., and Hunter, K. A.: Aerosol iron deposition to the surface ocean: modes of iron supply and biological responses, Mar. Chem., 120, 128–143, doi:10.1016/j.marchem.2009.01.008, 2010.

Buesseler, K. O., Andrews, J. E., Pike, S. M., and Charette, M. A.: The effects of iron fertilization on carbon sequestration in the Southern Ocean, Science, 30, 414–417, 2004.

Buesseler, K. O., Doney, S. C., Karl, D. M., Boyd, P. W., Caldeira, K., Chai, F., Coale, K. H., de Baar, H. J. W., Falkowski, P. G., Johnson, K. S., Lampitt, R. S., Michaels, A. F., Naqvi, S. W. A., Smetacek, V., Takeda, S., and Watson, A. J.: Ocean iron fertilization-moving forward in a sea of uncertainty, Science, 319, p. 162, 2008.

Cassar, N., Bender, M. L., Barnett, B. A., Fan, S., Moxim, W. J., Levy, H. L., and Tilbrook, B.: The Southern Ocean biological response to aeolian iron deposition, Science, 317, 1067–1070, 2007.

Chin, M., Chu, A., Levy, R., Remer, L., Kaufman, Y., Holben, B., Eck, T., Ginoux, P., and Gao, O.: Aerosol distribution in the Northern Hemisphere during ACE-Asia: results from global model, satellite observations, and sunphotometer measurements, J. Geophys. Res., 109, D23S90, doi:10.1029/2004JD004829, 2004.

Cloern, J. E., Grenz, C., and Vidergar-Lucas, L.: An empirical model of the phytoplankton chlorophyll: carbon ratio-the conversion factor between productivity and growth rate, Limnol. Oceanogr., 40, 1313–1321, 1995.

de Baar, H. J. W., de Jong, J. T. M., Bakker, D. C. E., Bettina, M. L., Cornelis, V., Bathmann, U., and Smetacek, V.: Importance of iron for plankton blooms and carbon dioxide drawdown in the Southern Ocean, Nature, 373, 412–415, 1995.

de Baar, H. J. W., Gerringa, L. J. A., Laan, P., and Timmermans, K. R.: Efficiency of carbon removal per added iron in ocean iron fertilization, Mar. Ecol-Prog. Ser., 364, 269–282, 2008.

de Boyer Montégut, C., Madec, G., Fischer, A. S., Lazar, A., and Iudicone, D.: Mixed layer depth over the global ocean: an examination of profile data and a profile-based climatology, J. Geophys. Res., 109, C12003, doi:10.1029/2004JC002378, 2004.

Delmonte, B., Petit, J. R., Andersen, K. K., Basile-Doelsch, I., Maggi, V., and Lipenkov, V. Y.: Dust size evidence for opposite regional atmospheric circulation changes over east Antarctica during the last climatic transition, Clim. Dynam., 23, 427–438, 2004.

Denman, K. L.: Climate change, ocean processes and ocean iron fertilization, Mar. Ecol-Prog. Ser., 364, 219–225, doi:10.3354/meps07542, 2008.

Dogliotti, A. I., Schloss, I. R., Almandoz, G. O., and Gagliardini, D. A.: Evaluation of SeaWiFS and MODIS chlorophyll-*a* products in the Argentinean Patagonian Continental Shelf (38° S–55° S), Int. J. Remote Sens., 1, 251–273, 2009.

Duce, R. A. and Tindale, N. W.: Atmospheric transport of iron and its deposition in the ocean, Limnol. Oceanogr., 36, 1715–1726, 1991.

Erickson, D. J., Hernandez, J. L., Ginoux, P., Gregg, W. W., McClain, C., and Christian, J.: Atmospheric iron delivery and surface ocean biological activity in the Southern Ocean and Patagonian region, Geophys. Res. Lett., 30(12), 1–4, doi:10.1029/2003GL017241, 2003.

Evans, M. J. and Jacob, D. J.: Impact of new laboratory studies of N_2O_5 hydrolysis on global model budgets of tropospheric nitrogen oxides, ozone, and OH, Geophys. Res. Lett., 32, L09813, doi:10.1029/2005GL022469, 2005.

Fairlie, T. D., Jacob, D. J., and Rokjin, R. J.: The impact of transpacific transport of mineral dust in the United States, Atmos. Environ., 41, 1251–1266, 2007.

Fung, I. Y., Meyn, S. K., Tegen, I., Doney, S. C., John, J. G., and Bishop, J. K. B.: Iron supply and demand in the upper ocean, Global Biogeochem. Cy., 14, 281–295, 2000.

Gabric, A. J., Cropp, R., Ayers, G. P., McTainsh, G., and Braddock, R.: Coupling between cycles of phytoplankton biomass and aerosol optical depth as derived from SeaWiFS time series in the Subantarctic Southern Ocean, Geophys. Res. Lett., 29(7), 1112, doi:10.1029/2001GL013545, 2002.

Gallegos, C. L. and Vant, W. N.: An incubation procedure for estimating carbon-to-chlorophyll ratios and growth-irradiance relationships of estuarine phytoplankton, Mar. Ecol-Prog. Ser., 138, 275–291, 1996.

Gassó, S. and Stein, A. F.: Does dust from Patagonia reach the sub-Antarctic Atlantic Ocean?, Geophys. Res. Lett., 34, L01801, doi:10.1029/2006GL027693, 2007.

Gassó, S., Stein, A., Marino, F., Castellano, E., Udisti, R., and Ceratto, J.: A combined observational and modeling approach to study modern dust transport from the Patagonia desert to East Antarctica, Atmos. Chem. Phys., 10, 8287–8303, doi:10.5194/acp-10-8287-2010, 2010.

Geist, H. J. and Lambin, E. F.: Dynamic causal patterns of desertification, Bioscience, 54(9), 817–829, 2004.

Ginoux, P., Chin, M., Tegen, I., Prospero, J. M., Holben, B., Dubovik, O., and Lin, S.-J.: Sources and distributions of dust aerosols simulated with the GOCART model, J. Geophys. Res., 106, 20255–20273, 2001.

Gregg, W. W. and Casey, N. W.: Global and regional evaluation of the SeaWiFS chlorophyll data set, Remote Sens. Environ., 93, 463–479, 2004.

Heald, C. L., Jacob, D. J., Jones, D. B. A., Palmer, P. I., Logan, J. A., Streets, D. G., Sachse, G. W., Gille, J. C., Hoffman, R. N., and Nehrkorn, T.: Comparative inverse analysis of satellite (MOPITT) and aircraft (TRACE-P) observations to estimate Asian sources of carbon monoxide, J. Geophys. Res., 109, D23306, doi:10.1029/2004JD005185, 2004.

Hutchins, D. A., Witter, A. E., Butler, A., and Luther, G. W.: Competition among marine phytoplankton for different chelated iron species, Nature, 400, 858–861, 1999.

Ito, A. and Kawamiya, M.: Potential impact of ocean ecosystem changes due to global warming on marine organic carbon aerosols, Global Biogeochem. Cy., 24, GB1012, doi:10.1029/2009GB003559, 2010.

Jickells, T. D., An, Z. S., Andersen, K. K., Baker, A. R., Bergametti, G., Brooks, N., Cao, J. J., Boyd, P. W., Duce, R. A., Hunter, K. A., Kawahata, H., Kubilay, N., LaRoche, J., Liss, P. S., Mahowald, N., Prospero, J. M., Ridgwell, A. J., Tegen, I., and Torres, R.: Global iron connections between desert dust, ocean biogeochemistry, and climate, Science, 308, 67–71, 2005.

Jin, X., Gruber, N., Frenzel, H., Doney, S. C., and McWilliams, J. C.: The impact on atmospheric CO_2 of iron fertilization induced changes in the ocean's biological pump, Biogeosciences, 5, 385–406, doi:10.5194/bg-5-385-2008, 2008.

Johnson, M. S., Meskhidze, N., Solmon, F., Gassó, S., Chuang, P. Y., Gaiero, D. M., Yantosca, R. M., Wu, S., Wang, Y., and Carouge, C.: Modeling dust and soluble iron deposition to the South Atlantic Ocean, J. Geophys. Res., 115, D15202, doi:10.1029/2009JD013311, 2010.

Kaufman, Y. J., Tanré, D., Remer, L. A., Vermote, E., Chu, A., and Holben, B. N.: Operational remote sensing of tropospheric aerosol over land from EOS moderate resolution imaging spectroradiometer, J. Geophys. Res., 102, 17051–17067, 1997.

Korb, R. E., Whitehouse, M. J., and Ward, P.: SeaWiFS in the southern ocean: spatial and temporal variability in phytoplankton biomass around South Georgia, Deep-Sea Res. Pt. II, 51, 99–116, 2004.

Krinner, G. and Genthon, C.: Tropospheric transport of continental tracers towards Antarctica under varying climatic conditions, Tellus, 53, 54–70, 2003.

Krinner, G., Petit, J. R., and Delmonte, B.: Altitude of atmospheric tracer transport towards Antarctica in present and glacial climate, Quaternary Sci. Rev., 29, 274–284, 2010.

Lambert, F., Delmonte, B., Petit, J. R., Bigler, M., Kaufmann, P. R., Hutterli, M. A., Stocker, T. F., Ruth, U., Steffensen, J. P., and Maggi, V.: Dust-climate coupling over the past 800 000 years from the EPICA Dome C ice core, Nature, 452, 616–619, doi:10.1038/nature06763, 2008.

Lancelot, C., de Montety, A., Goosse, H., Becquevort, S., Schoemann, V., Pasquer, B., and Vancoppenolle, M.: Spatial distribution of the iron supply to phytoplankton in the Southern Ocean: a model study, Biogeosciences, 6, 2861–2878, doi:10.5194/bg-6-2861-2009, 2009.

Li, F., Ginoux, P., and Ramaswamy, V.: Distribution, transport, and deposition of mineral dust in the Southern Ocean and Antarctica: contribution of major sources, J. Geophys. Res., 113, D10207, doi:10.1029/2007JD009190, 2008.

Li, F., Ginoux, P., and Ramaswamy, V.: Transport of Patagonian dust to Antarctica, J. Geophys. Res., 115, D18217, doi:10.1029/2009JD012356, 2010.

Liang, Q., Jaegle, L., and Wallace, J. M.: Meteorological indices for Asian outflow and transpacific transport on daily to interannual timescales, J. Geophys. Res., 110, D18308, doi:10.1029/2005JD005788, 2005.

Liu, Z., Vaughan, M., Winker, D., Kittaka, C., Getzewich, B., Kuehn, R., Omar, A., Powell, K., Trepte, C., and Hostetler, C.: The CALIPSO lidar cloud and aerosol discrimination: version 2 algorithm and initial assessment of performance, J. Atmos. Ocean. Tech., 26, 1198–1213, doi:10.1175/2009JTECHA1229.1, 2009.

Löscher, B. M., de Baar, H. J. W., de Jong, J. T. M., Veth, C., and Dehairs, F.: The distribution of Fe in the Antarctic circumpolar current, Deep-Sea Res. Pt. II, 44, 143–187, 1997.

Mackie, D. S., Boyd, P. W., McTainsh, G. H., Tindale, N. W., Westberry, T. K., and Hunter, K. A.: Biogeochemistry of iron in Australian dust: from eolian uplift to marine uptake, Geochem. Geophy. Geosy., 9, Q03Q08, doi:10.1029/2007GC001813, 2008.

Martin, J. H. and Fitzwater, S. E.: Iron-deficiency limits phytoplankton growth in the Northeast Pacific Subarctic, Nature, 331, 341–343, 1988.

Martin, J. H. and Gordon, R. M.: Northeast Pacific iron distributions in relation to phytoplankton productivity, Deep-Sea Res., 35, 177–196, 1988.

Martin, J. H.: Glacial-interglacial CO$_2$ change: the iron hypothesis, Paleoceanography, 5, 1–13 1990.

McConnell, J. R., Aristarain, A. J., Banta, J. R., Edwards, P. R., and Simões, J. C.: 20th-Century doubling in dust archived in an Antarctic Peninsula ice core parallels climate change and desertification in South America, P. Natl. Acad. Sci., 104(14), 5743–5748, 2007.

Meredith, M. P., Watkins, J. L., Murphy, E. J., Cunningham, N. J., Wood, A. G., Korb, R.,

Title Page
Abstract Introduction
Conclusions References
Tables Figures
◀| |▶
◀ ▶
Back Close
Full Screen / Esc
Printer-friendly Version
Interactive Discussion

Whitehouse, M. J., Thorpe, S. E., and Vivier, F.: An anticyclonic circulation above the Northwest Georgia Rise, Southern Ocean, Geophys. Res. Lett., 30(20), 2061, doi:10.1029/2003GL018039, 2003.

Meskhidze, N., Chameides, W. L., Nenes, A., and Chen, G.: Iron mobilization in mineral dust: can anthropogenic SO_2 emissions affect ocean productivity?, Geophys. Res. Lett., 30(21), 2085, doi:10.1029/2003GL018035, 2003.

Meskhidze, N., Chameides, W. L., and Nenes, A.: Dust and pollution: a recipe for enhanced ocean fertilization?, J. Geophys. Res., 110, D03301, doi:10.1029/2004JD005082, 2005.

Meskhidze, N., Nenes, A., Chameides, W. L., Luo, C., and Mahowald, N.: Atlantic Southern Ocean productivity: Fertilization from above or below?, Global Biogeochem. Cy., 21, GB2006, doi:10.1029/2006GB002711, 2007.

Omar, A., Winker, D. M., Kittaka, C., Vaughan, M. A., Liu, Z., Hu, Y., Trepte, C. R., Rogers, R. R., Ferrare, R. A., Lee, K., Kuehn, R. E., and Hostetler, C. A.: The CALIPSO automated aerosol classification and lidar ratio selection algorithm, J. Atmos. Ocean. Tech., 26, 1994–2014, doi:10.1175/2009JTECHA1231.1, 2009.

O'Reilly, J. E., Maritorena, S., Mitchell, B. G., Siegel, D. A., Carder, K. L., Garver, S. A., Kahru, M., and McClain, C.: Ocean color chlorophyll algorithms for SeaWiFS, J. Geophys. Res., 103(C11), 24937–24953, doi:10.1029/98JC02160, 1988.

Park, R. J., Jacob, D. J., Field, B. D., Yantosca, R. M., and Chin, M.: Natural and transboundary pollution influences on sulfate-nitrate-ammonium aerosols in the United States: implications for policy, J. Geophys. Res., 109, D15204, doi:10.1029/2003JD004473, 2004.

Petit, J. R., Jouzel, J., Raynaud, D., Barkov, N. I., Barnola, J.-M., Basile, I., Bender, M., Chappellaz, J., Davis, M., Delaygue, G., Delmotte, M., Kotlyakov, V. M., Legrand, M., Lipenkov, V. Y., Lorius, C., Pepin, L., Ritz, C., Saltzman, E., and Stievenard, M.: Climate and atmospheric history of the past 420 000 years from the Vostok ice core, Antarctica, Nature, 399, 429–436, 1999.

Prospero, J. M., Ginoux, P., Torres, O., and Nicholson, S. E.: Environmental characterization of global sources of atmospheric soil dust identified with the Nimbus 7 Total Ozone Mapping Spectrometer (TOMS) absorbing aerosol product, Rev. Geophys., 40(3), 1002, doi:10.1029/2000RG000095, 2002.

Raiswell, R., Benning, L. G., Tranter, M., and Tulaczyk, S.: Bioavailable iron in the Southern Ocea: the significance of the iceberg conveyor belt, Geochemical Transactions, 9(7), doi:10.1186/1467-4866-9-7, 2008.

Remer, L. A., Kaufman, Y. J., Mattoo, S., Martins, J. V., Ichoku, C., Levy, R. C., Kleidman, R. G., Tanré, D., Chu, D. A., Li, R. R., Eck, T. F., Vermote, E., and Holben, B. N.: The MODIS algorithm, products and validation, J. Atmos. Sci., 62, 947–973, doi:10.1175/JAS3385.1, 2005.

Romero, S. I., Piola, A. R., Charo, M., and Garcia, C. A. E.: Chlorophyll-*a* variability off Patagonia based on SeaWiFS data, J. Geophys. Res., 111, C05021, doi:10.1029/2005JC003244, 2006.

Sarmiento, J. L., Gruber, N., Brzezinski, M. A., and Dunne, J. P.: High-latitude controls of thermocline nutrients and low latitude biological productivity, Nature, 427, 56–60, 2004.

Sarthou, G., Timmermans, K. R., Blain, S., and Treguer, P.: Growth physiology and fate of diatoms in the ocean: a review, J. Sea Res., 53, 25–42, 2005.

Solmon, F., Chuang, P. Y., Meskhidze, N., and Chen, Y.: Acidic processing of mineral dust iron by anthropogenic compounds over the North Pacific Ocean, J. Geophys. Res., 114, D02305, doi:10.1029/2008JD010417, 2009.

Strong, A., Chisholm, S., Miller, C., and Cullen, J.: Ocean fertilization: time to move on, Nature, 461(17), 347–348, 2009.

Tanré, D., Kaufman, Y. J., Herman, M., and Mattoo, S.: Remote sensing of aerosol properties over oceans using the MODIS/EOS spectral radiances, J. Geophys. Res., 102(D14), 16971–16988, 1997.

Tsuda, A. S., Takeda, S., Saito, H., Nishioka, J., Nojiri, Y., Kudo, I., Kiyosawa, H., Shiomoto, A., Imai, K., Ono, T., Shimamoto, A., Tsumune, D., Yoshimura, T., Aono, T., Hinuma, A., Kinugasa, M., Suzuki, K., Sohrin, Y., Noiri, Y., Tani, H., Deguchi, Y., Tsurushima, N., Ogawa, H., Fukami, K., Kuma, K., and Saino, T.: A mesoscale iron enrichment in the Western Subarctic Pacific induces a large centric diatom bloom, Science, 300, 958–961, 2003.

Twining, B. S., Baines, S. B., Fisher, N. S., and Landry, M. R.: Cellular iron contents of plankton during the Southern Ocean Iron Experiment (SOFeX), Deep-Sea Res. Pt. I, 51, 1827–1850, 2004.

Vaughan, M., Young, S., Winker, D., Powell, K., Omar, A., Liu, Z., Hu, Y., and Hostetler, C.: Fully automated analysis of space-based lidar data: an overview of the CALIPSO retrieval algorithms and data products, Bba. Lib., 5575, doi:10.1117/12.572024, 2004.

Wagener, T., Guieu, C., Losno, R., Bonnet, S., and Mahowald, N.: Revisiting atmospheric dust export to the Southern Hemisphere ocean: biogeochemical implications, Global Biogeochem. Cy., 22, GB2006, doi:10.1029/2007GB002984, 2008.

Watson, A. J., Bakker, D. C. E., Ridgwell, A. J., Boyd, P. W., and Law, C. S.: Effect of iron supply on Southern Ocean CO_2 uptake and implications for glacial atmospheric CO_2, Nature, 407, 730–733, 2000.

Yang, Y. Q., Hou, Q., Zhou, C. H., Liu, H. L., Wang, Y. Q., and Niu, T.: Sand/dust storm processes in Northeast Asia and associated large-scale circulations, Atmos. Chem. Phys., 8, 25–33, doi:10.5194/acp-8-25-2008, 2008.

Young, S., and Vaughan, M.: The retrieval of profiles of particulate extinction from Cloud Aerosol Lidar Infrared Pathfinder Satellite Observation (CALIPSO) data: algorithm description, J. Atmos. Oceanic Technol., 26, 1105–1119, 2009.

Yu, H., Chin, M., Winker, D. M., Omar, A. H., Liu, Z., Kittaka, C., and Diehl, T.: Global view of aerosol vertical distributions from CALIPSO lidar measurements and GOCART simulations: regional and seasonal variations, J. Geophys. Res., 115, D00H30, doi:10.1029/2009JD013364, 2010.

Zender, C. S., Newmann, D., and Torres, O.: Spatial heterogeneity in aeolian erodibility: uniform, topographic, geomorphic, and hydrologic hypotheses, J. Geophys. Res., 108(D17), 4543, doi:10.1029/2002JD003039, 2003.

Zhuang, G., Yi, Z., Duce, R. A., and Brown, P. R.: Link between iron and sulphur cycles suggested by detection of Fe(II) in remote marine aerosols, Nature, 355, 537–539, 1992.

Table 1. Variables with corresponding values and (uncertainties) used in Eq. (2).

Variable	Value	Source
sol-Fe (mol m^{-2} day^{-1})	GEOS-Chem/DFeS	Solmon et al. (2009)
C:Fe (mol mol^{-1})	30 000 (±24 000)	de Baar et al. (2008), Sarthou et al. (2005), Twining et al. (2004)
Chl-*a*:C (mg mg^{-1})	1/30 (1/15–1/100)	Gallegos and Vant (1996), Cloern et al. (1995)
Mixed layer depth (m)	Climatological monthly-average	de Boyer Montégut (2004)

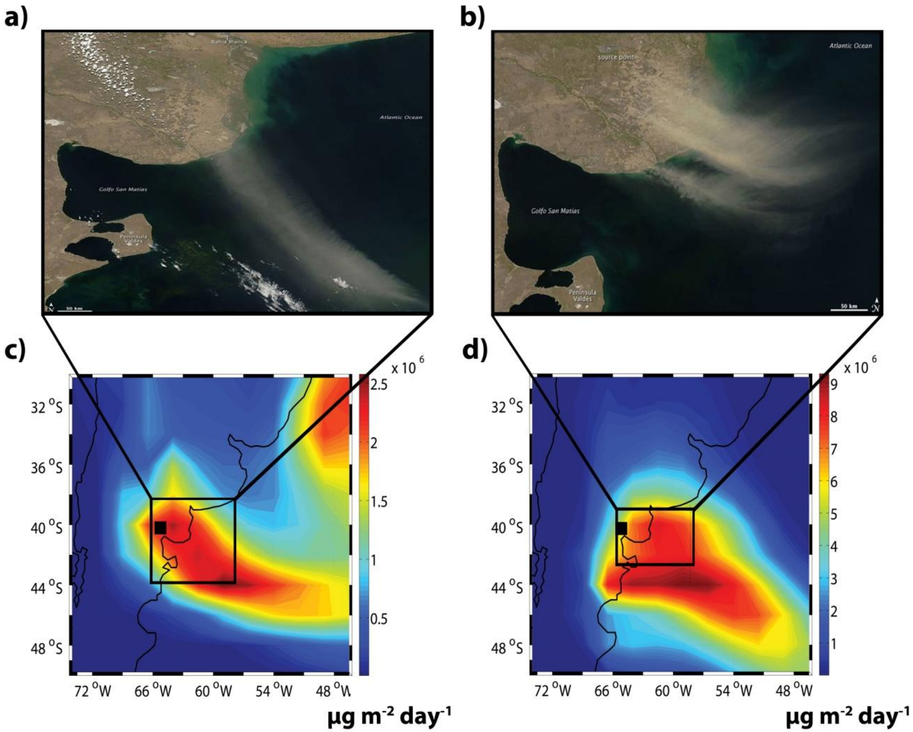

Fig. 1. Aqua MODIS real-time imagery and GEOS-Chem-predicted column dust concentrations ($\mu g\,m^{-2}\,day^{-1}$) of Patagonian dust plumes advecting off the coast of South America on **(a, c)** 23 January 2009 and **(b, d)** 17 February 2009, respectively. The black square indicates the location of San Antonio Oeste (40.8° S, 65.1° W).

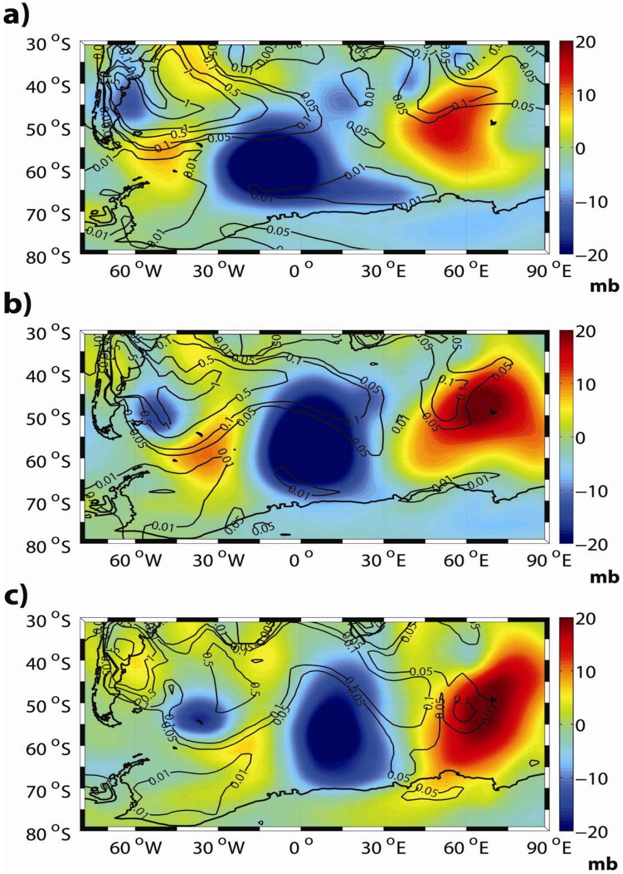

Fig. 2. GEOS-Chem-predicted daily dust burden (g m^{-2}) (contour lines) and sea level pressure anomalies (SLPAs) (mb) over the SAO for **(a)** 23 January, **(b)** 24 January, and **(c)** 25 January 2009. Cold colors indicate negative SLPA (low pressure systems) and warm colors display high pressure systems.

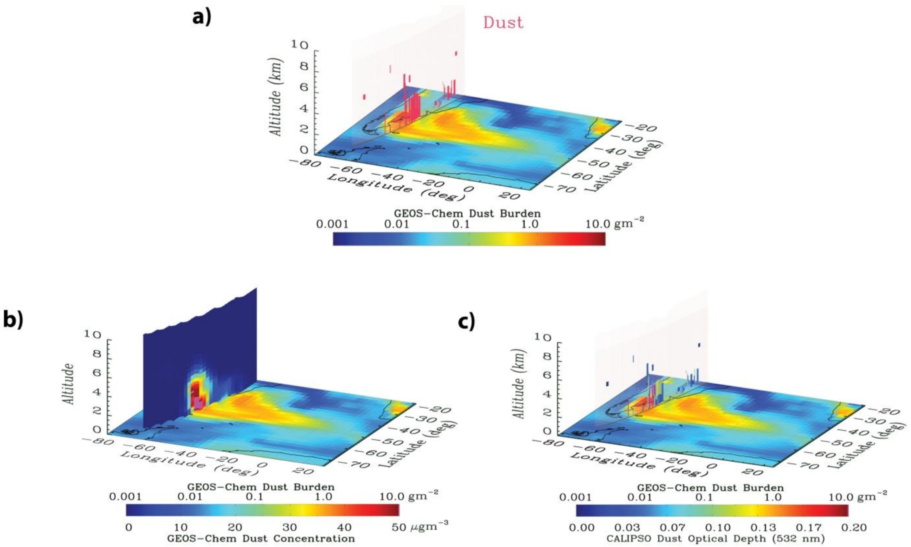

Fig. 3. GEOS-Chem-predicted dust burden (g m^{-2}) with overlaid **(a)** CALIPSO retrievals of dust aerosol layers, **(b)** model-predicted vertical cross-section of dust concentration (µg m^{-3}) along the CALIPSO orbit track and **(c)** CALIPSO dust layer AOD at 532 nm on 23 January 2009. Model cross-section calculations are conducted along the CALIPSO orbital track beginning at 4:28:59 UTC (V3-01.2009-01-23T04-28-59ZN).

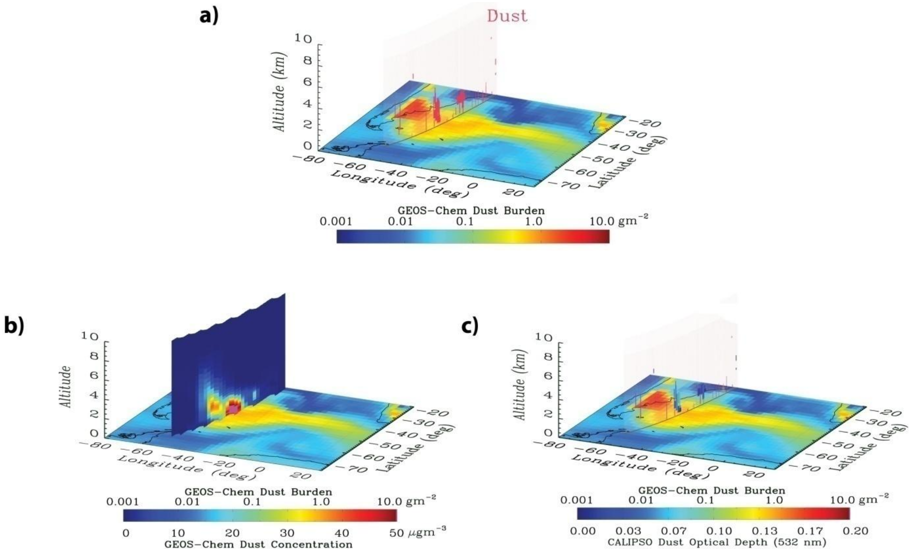

Fig. 4. Same as Fig. 3 but for 24 January 2009 and the CALIPSO orbital track beginning at 03:33:27 UTC (V3-01.2009-01-24T03-33-27ZN).

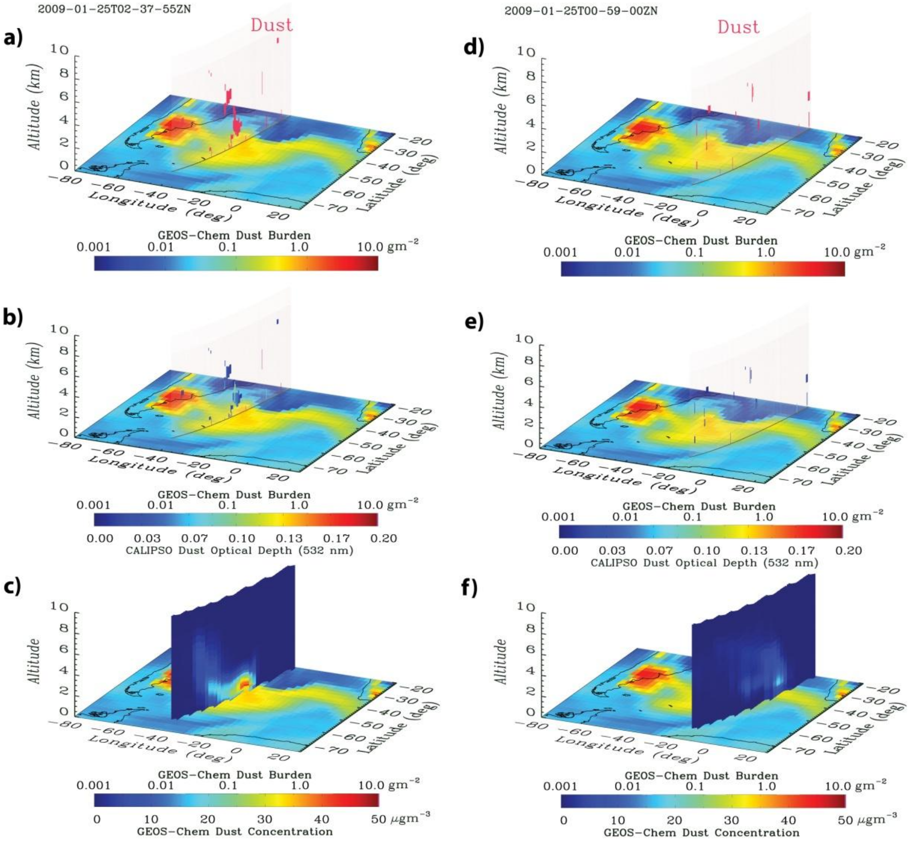

Fig. 5. GEOS-Chem-predicted dust burden (g m^{-2}) on 25 January 2009 overlaid with the CALIPSO orbital track beginning at 02:37:55 UTC (V3-01.2009-01-25T02-37-55ZN) (left column) and 00:59:00 UTC (V3-01.2009-01-25T00-59-00ZN) (right column) **(a, d)** CALIPSO retrievals of dust aerosol layers, **(b, e)** CALIPSO dust layer AOD at 532 nm, and **(c, f)** model-predicted vertical cross-section of dust concentration (µg m^{-3}) along the CALIPSO orbit tracks.

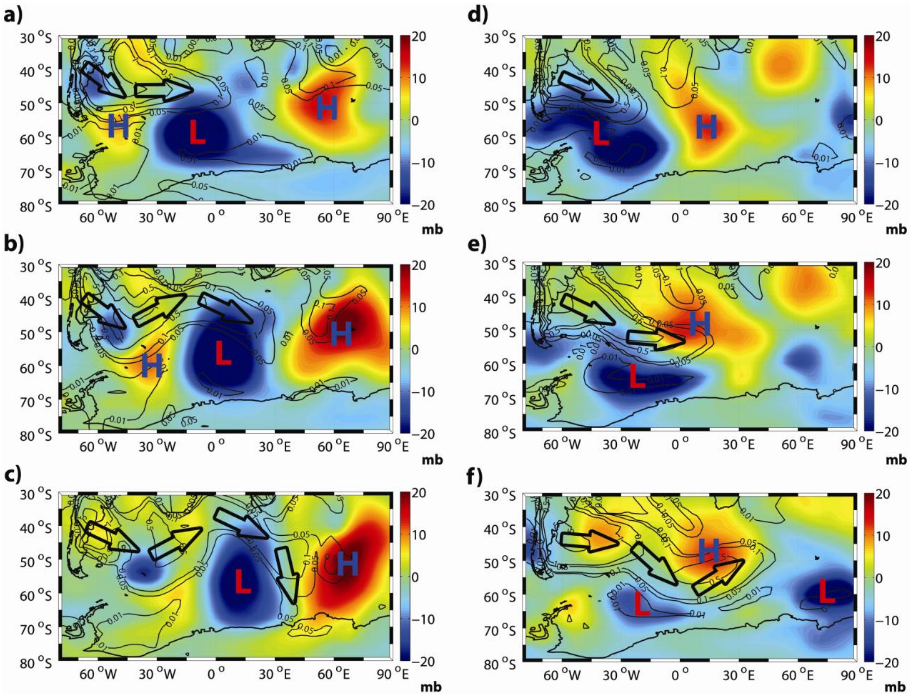

Fig. 6. GEOS-Chem-predicted dust burden (g m^{-2}) (contour lines) and sea level pressure anomalies (SLPAs) (mb) over the SAO for **(a–c)** 23–25 January 2009 and **(d–f)** 13–15 February 2009. Arrows are for the visual aid for the general transport pathway of Patagonian dust. Low and high pressure anomalies are shown by symbols of L and H, respectively.

Title Page
Abstract | Introduction
Conclusions | References
Tables | Figures
◀| |▶
◀ ▶
Back | Close
Full Screen / Esc

Printer-friendly Version

Interactive Discussion

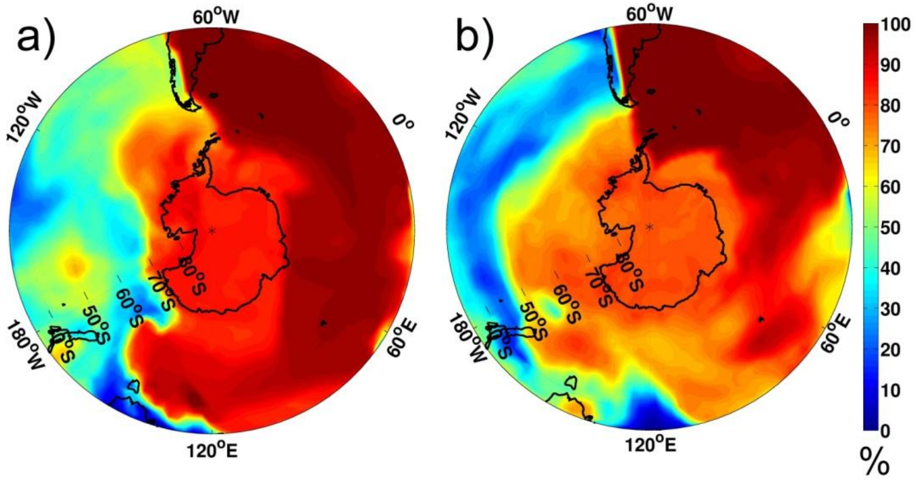

Fig. 7. The 8-day averaged GEOS-Chem-predicted percent contributions of Patagonian dust sources to total mineral dust deposition in the HNLC waters of the SO for the **(a)** J23 and **(b)** F11 dust episodes.

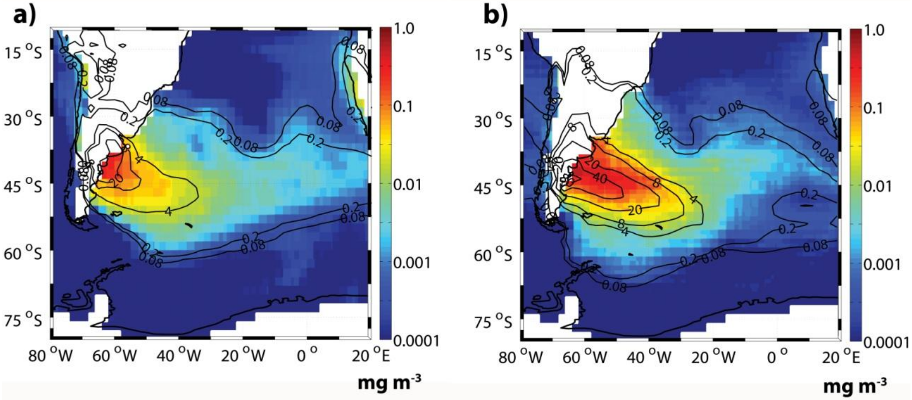

Fig. 8. GEOS-Chem/DFeS-simulated total sol-Fe fluxes (µg m^{-2}) (contour lines) and predicted [Chl-*a*] increases (Δ[Chl-*a*]$_{\mathrm{pred}}$) (mg m^{-3}) for the **(a)** J23 and **(b)** F11 dust episodes.

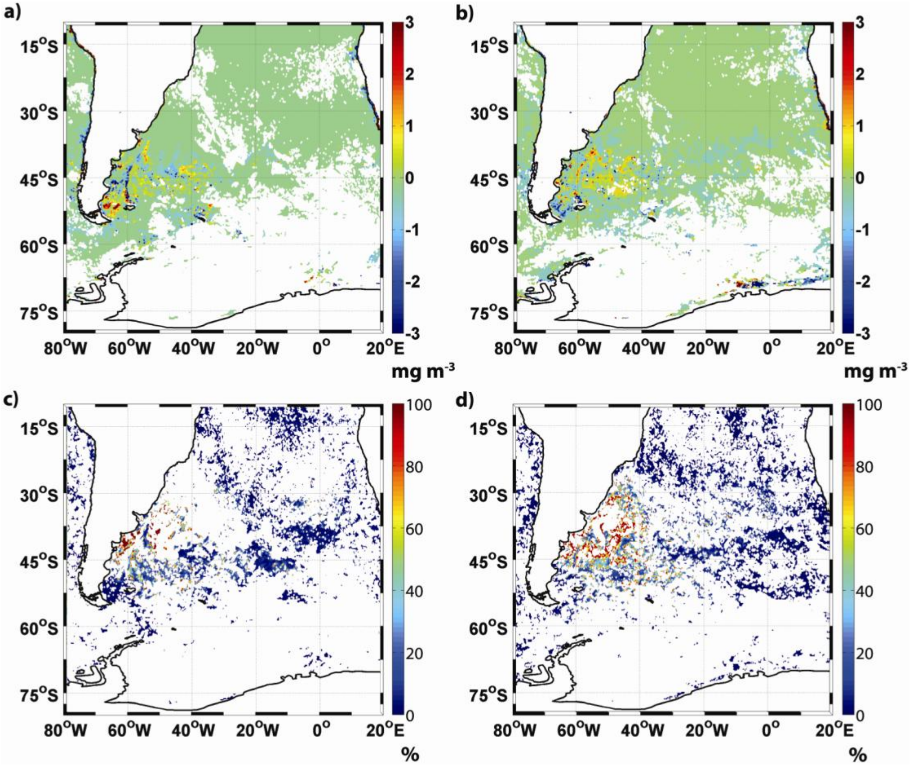

Fig. 9. Differences in SeaWiFS remotely-sensed 8-day averaged [Chl-*a*] (Δ[Chl-*a*]$_{\text{obs}}$) (mg m^{-3}) and the percent ratio of Δ[Chl-*a*]$_{\text{pred}}$/Δ[Chl-*a*]$_{\text{obs}}$ for the **(a, c)** J23 and **(b, d)** F11 dust episodes, respectively. The Δ[Chl-*a*]$_{\text{obs}}$ for J23 and F11 episodes are calculated by subtracting 23–30 January averages from 15–22 January 2009 and 11–18 February averages from 3–10 February 2009, respectively.

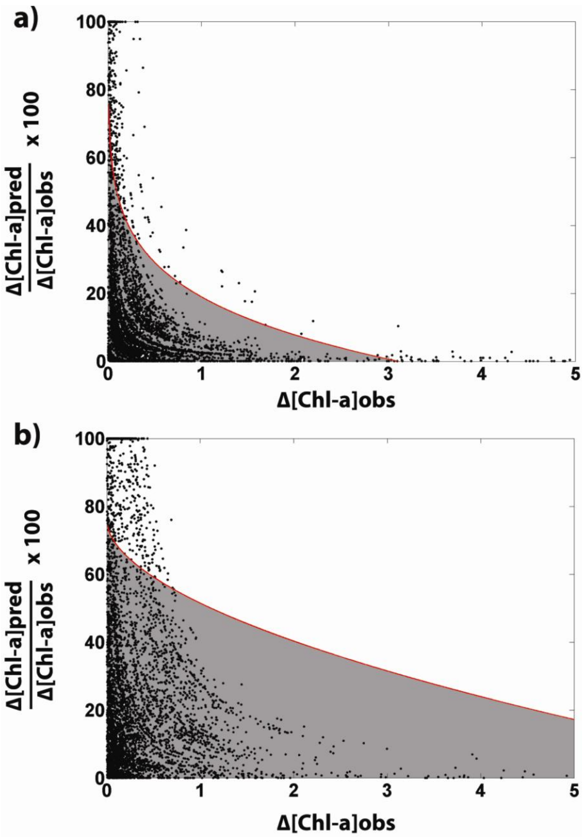

Fig. 10. Percent ratio of $\Delta[\text{Chl-}a]_{\text{pred}}/\Delta[\text{Chl-}a]_{\text{obs}}$ for the grid cells with positive values of remotely-sensed 8-day averaged [Chl-*a*] differences (after the storm minus before) for the **(a)** J23 and **(b)** F11 dust episodes. Black dots depict the grid cells located in the HNLC regions of the SAO. Red solid line represents the line of best-fit for the ratios of $\Delta[\text{Chl-}a]_{\text{pred}}/\Delta[\text{Chl-}a]_{\text{obs}}$ when uncertainties in $\Delta[\text{Chl-}a]_{\text{pred}}$ calculations are included. See text for more details.